SAND2018-1450C

2018-01-1252

Spark Assist for CA50 Control and Improved Robustness in a Premixed LTGC Engine – Effects of Equivalence Ratio and Intake Boost

Author, co-author (Do NOT enter this information. It will be pulled from participant tab in MyTechZone)

Affiliation (Do NOT enter this information. It will be pulled from participant tab in MyTechZone)

Abstract

Low-temperature gasoline combustion (LTGC) engines can deliver high efficiencies, with ultra-low emissions of nitrogen oxides (NO_x) and particulate matter (PM). However, controlling the combustion timing and maintaining robust operation remains a challenge for LTGC engines. One promising technique to overcoming these challenges is spark assist (SA). In this work, well-controlled, fully premixed experiments are performed in a single-cylinder LTGC research engine at 1200 rpm using a cylinder head modified to accommodate a spark plug. Compression ratios (CR) of 16:1 and 14:1 were used during the experiments. Two different fuels were also tested, with properties representative of premium- and regular-grade market gasolines. SA was found to work well for both CRs and fuels. The equivalence ratio (ϕ) limits and the effect of intake-pressure boost on the ability of SA to compensate for a reduced T_{in} were studied. For the conditions studied, ϕ=0.42 was found to be most effective for SA. At lower equivalence ratios the flame propagation was too weak, whereas ϕ=0.45 was closer to the CI knock/stability limit, which resulted in a smaller range of CA50 control and T_{in} compensation. At ϕ=0.42, SA worked well from P_{in}= 1.0 to 1.6 bar, but the range of effective T_{in} compensation dropped progressively with boost from 21°C at P_{in} = 1.0 bar to the equivalent of 12°C at P_{in} = 1.6 bar. The amount of control authority using SA was demonstrated by varying the spark timing, advancing CA50 to the onset of strong knocking and then retarding CA50 to near misfire. SA provided good control, however the CA50 control range decreased from 7.2° CA at P_{in}=1.0 bar to 4.2° CA at P_{in}=1.6 bar. For all intake pressures at these well-mixed conditions, NO_x emissions for SA were less than for compression ignition only, and all were below the US-2010 Heavy Duty limit.

Introduction

Low-temperature gasoline combustion (LTGC) engines can deliver high efficiencies, with ultra-low emissions of nitrogen oxides (NO_x) and particulate matter (PM). However, controlling the combustion timing and maintaining robust operation remains a challenge for LTGC engines. The most fundamental form of LTGC, homogeneous charge compression ignition (HCCI), occurs when a fully premixed fuel and air mixture are compressed to the point of autoignition by the piston motion, with chemical kinetics controlling the start of combustion. These kinetic rates can be sensitive to the in-cylinder conditions, which leads to difficulty in keeping the combustion phasing between the allowable limits of misfire and knocking.

One promising technique to overcoming these challenges is spark assist (SA). With SA-LTGC, a spark initiates a flame kernel and the subsequent flame propagation compresses the unburned mixture, increasing its temperature and pressure and ultimately, driving the main charge into autoignition. Because this flame combustion compresses the remaining unburned mixture to a greater extent than the piston motion would by itself, it can induce combustion at conditions that would not otherwise autoignite. Thus, it reduces the intake temperatures or amount of hot residuals required to maintain a desired combustion phasing and acceptable combustion stability. Similarly, this compression heating can also compensate for the decrease in oxygen concentration when recirculated exhaust gasses (EGR) are used, so higher levels of EGR can be tolerated. Perhaps most importantly, the spark acts as a trigger for the start of combustion, allowing for direct control over the combustion phasing by varying the spark timing instead of relying on chemical kinetics alone to initiate combustion. However, despite these advantages, there are limitations to the operating conditions for which SA will be effective. For instance, the equivalence ratio and charge temperature must be high enough to allow for adequate flame propagation, yet the compressed-gas temperature and pressure must remain low enough so that autoignition doesn't occur prior to the flame propagation [1].

LTGC engines typically operate quite dilute to keep combustion temperatures low and to manage the high rates of heat release that can occur with compression ignition of a well-mixed charge. Charge dilution is generally accomplished by using some combination of excess air, EGR, and/or retained residuals. For this reason, it is often convenient to compare mixtures with the same supplied energy content per charge mass by using a charge-mass based equivalence ratio (ϕ_m) to describe the mixture stoichiometry.

$$\phi_m = \frac{\left({}^{F}/_{C}\right)}{\left({}^{F}/_{A}\right)_{stoich.}} \qquad (1)$$

Where F/C is the ratio of fuel mass to the total charge mass, and $(F/A)_{stoich.}$ is the fuel-to-air mass ratio for a stoichiometric mixture. It is important to note that when there are no exhaust or residual gases, ϕ_m is the same as the conventional air-based equivalence ratio (ϕ).

At naturally aspirated conditions and for typical gasoline fuels, compression ratios, and equivalence ratios used for LTGC, the autoignition temperature is higher than what can be achieved by compression from the piston with ambient intake conditions, and some additional heat is required. Using port fuel injection (PFI) or early direct injection (DI) further adds to the heating requirements due to the charge cooling effect from the vaporizing fuel. In practice, the additional heat can be obtained by heating the intake air or utilizing valve timing strategies to retain or rebreathe hot residuals [2-6].

Several authors have investigated various aspects of naturally aspirated SA-LTGC; Zigler et al**.** [5] performed a spark-assisted HCCI study in a single cylinder optically accessible research engine with a compression ratio (CR) of 10:1. Preheated air and PFI were used for charge preparation, without trapping of residual gasses. The fuel used was indolene, an E0 reference gasoline (97.4 RON, 88.3 MON). Intake temperatures and spark timing were varied for equivalence ratios spanning from ϕ=0.38 to 0.62. At ϕ=0.38 optical imaging showed that a weak reaction front was present, with the heat release being too small to distinguish from the measured pressure trace for this condition. Overall, it was found that SA was able to affect the heat release rate, combustion phasing, and engine stability at the conditions considered.

Persson et al. [3] also studied SA using a single-cylinder optical engine with PFI, but controlled the initial charge temperature by varying the amount of hot residuals retained in the cylinder. The CR used was 9:1, requiring a fuel with a lower octane number. The fuel blend chosen for the experiments comprised of 40% ethanol and 60% n-heptane (70 RON, 65 MON). The fuel properties were not included in the manuscript, but for comparison are inferred by utilizing the octane number measurements of ethanol and n-heptane fuel blends made by Foong et al. [7]. A spark timing sweep was performed at a low-load condition, with a high amount of retained hot residual gasses. During the sweep, the spark timing was advanced from 30 to 60 crank angle degrees (° CA) before top dead center (bTDC), advancing CA50 by 7.3° CA. The coefficient of variation (COV) of the indicated mean effective pressure (IMEP) was nearly constant around 4% until the spark timing was advanced beyond 55° CA bTDC, causing a rapid increase in cycle-to-cycle variation due to occasional misfires. For the misfired cycles, in-cylinder temperatures and turbulence levels at the time of the spark were thought to be too low to allow for flame propagation.

Manofsky-Olesky et al. [6, 8-10] performed several studies using a single-cylinder gasoline direct-injected engine with a CR=12.5:1, using residual gas trapping to provide sufficient heat for SA-LTGC. The fuel used was a research-quality gasoline with properties representing a regular-grade pump gasoline (Anti-knock index (AKI) =87), and it was injected into the cylinder early during the compression stroke. In one of the studies [8], baseline compression ignition only results at ϕ_m=0.38 were first obtained with a CA50 at 8° CA aTDC (considered to be a near optimal phasing for maximum thermal efficiency). Spark timing sweeps were then performed starting at 30° CA bTDC, and advancing the spark timing at 10° CA increments. For conditions without EGR, the CA50 could be advanced by 8° CA to occur at TDC. The corresponding spark timing for this condition occurred at about 90° CA bTDC; further spark advance up to 120° CA bTDC caused the combustion phasing to revert back to the HCCI baseline, indicating that the SA was no longer effective. A detailed three-dimensional simulation accompanying the experimental work showed that as the spark timing was advanced from the start of the sweep, the mixture became increasingly stratified with the local equivalence ratio in the region of the spark gap increasing from the base condition at ϕ_m=0.38 up to ϕ_m=0.80, which was thought to help facilitate spark-initiated flame combustion at early spark timings.

The results of the preceding paragraph suggest that the fuel, air, and residuals may not be completely premixed when utilizing an early-DI with advanced spark timings. However, when using an early-DI, even if the spark timing is later in the cycle, or for compression ignition without a spark, the mixture is still not likely to be well-mixed. In the literature, an early-DI fueling event is often said to provide a nearly homogenous mixture, but in fact a significant amount of compositional stratification remains. This was illustrated in the work by Dec et al. [11] who performed an experiment to understand the difference between fully premixed operation and early-DI fuel injection using a single-cylinder optical engine. To visualize the difference in fuel distribution for these two fueling strategies, Planar Laser Induced Fluorescence (PLIF) images were taken at the horizontal mid-plane of the charge, 40° CA bTDC for ϕ=0.40 during motored operation, using 3-pentanone as a fluorescent tracer. The left-hand image in Figure 1 shows that for fully premixed fueling there are only small variations in the image intensity due to naturally occurring thermal stratification (resulting from heat transfer and turbulent convection) [12]. However, for early-DI fueling (right-hand image), variations in image intensity are much larger, indicating that there are significant non-uniformities resulting from the early-DI fueling. These much greater non-uniformities for early-DI fueling are likely due to a combination of variations in fuel concentration combined with thermal effects of the DI-fueling (i.e. fuel vaporization cooling) in addition to the natural thermal stratification that occurs even with fully premixed fueling. Similar mixture and thermal inhomogeneities are also likely to occur with PFI [13, 14].

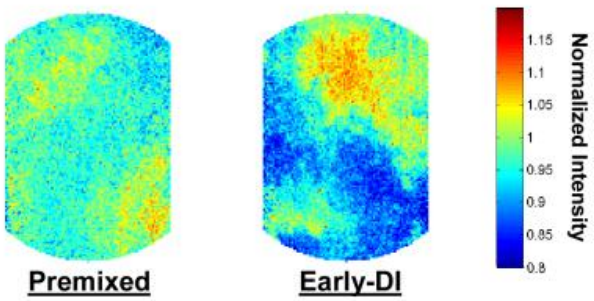

Figure 1. Single-shot PLIF images of 3-pentanone tracer mixed in the fuel for fully premixed and Early-DI fueling with ϕ=0.40, acquired at 40° CA bTDC in the mid-plane of the combustion chamber [11].

Furthermore, for engines that utilize valve timing strategies to retain hot residuals to supply the necessary heat for autoignition, there may be incomplete mixing between the hot residuals and the colder fuel-air mixtures that are inducted into the cylinder because of reduced intake flow velocities and turbulence that normally promote mixing. Another challenge with this heating strategy is that there is strong feedback from one cycle to the next, particularly during unstable conditions where a misfire or partial burn cycle may occur, so the residuals from the previous cycle may not be hot enough to initiate combustion in the following cycle [4]. Fuel distribution and incomplete mixing will also have an impact on combustion characteristics and emissions, making it difficult to interpret experimental results and determine fundamental limits.

The objective of the current work is to investigate the fundamental aspects of SA-LTGC, including the effects of equivalence ratio and intake pressure (simulating boosted operation), and the influence of moderate changes in compression ratio and fuel properties. Well-characterized conditions are maintained throughout the study by using a fueling system that provides a thoroughly premixed charge, electrically heating the intake air to hold steady intake temperatures (T_{in}), and using an external air compressor to provide steady intake pressures (P_{in}) from naturally aspirated to moderate boost levels [15, 16]. Holding the intake temperature and pressure is particularly important for collecting data near unstable conditions, to minimize the effects of partial-burn or misfire cycles when determining the combustion-stability limits. For each parameter investigated (equivalence ratio, intake pressure, etc.), data were first obtained for a baseline compression-ignition (CI) only case, then compared with data obtained using SA. To allow the spark-initiated flame to assist the CI, the autoignition reactivity is progressively reduced below that required for CI only by reducing T_{in} or adding EGR, while the spark timing is adjusted to maintain the same combustion phasing as the baseline CI only point. This procedure allows the potential of SA to compensate for reduced T_{in} or EGR addition to be determined for each condition. Additionally, for several conditions, the amount of combustion-timing control authority provided by SA is also assessed by varying the spark timing to change the 50% burn point (CA50) from heavy knocking (overly advanced CA50) to near misfire (overly retarded CA50).

After a description of the experimental facility and data acquisition techniques in the next section, the results of the study are presented in four parts:

1) An initial demonstration of SA-LTGC is presented for CR = 16:1, showing the ability of SA to compensate for reduced T_{in} and to control CA50.
2) The effects of changing the CR from 16:1 to 14:1 and the fuel from a 92 AKI certification gasoline to an 87 AKI regular E10 on the potential of SA.
3) A detailed investigation of SA-LTGC for naturally aspirated operation with CR=14:1 and regular E10, including the effects of equivalence ratio and a study of the reason for the low-T_{in} limit.
4) Intake pressure effects on SA-LTGC limits and performance, including emissions data.

Experimental Setup

Engine Facility

The LTGC/HCCI research engine used for this study was derived from a Cummins B-series six-cylinder diesel engine, which is a typical medium-duty diesel engine with a displacement of 0.98 liters per cylinder. As shown in the schematic of the engine facility in Figure 2a, the engine has been converted for single-cylinder operation by deactivating cylinders 1-5. The configuration of the engine and facility is nearly identical to those used in our previous studies involving intake pressure boost [17, 18], with the exception of the cylinder head, which has been modified to accommodate a spark plug as discussed below, and the geometry of the CR = 14:1 piston. Figures 2b and 2c show drawings of the CR = 14:1 and 16:1 pistons used in the active LTGC cylinder, respectively. The CR = 16:1 piston is the same one used in all previous studies, but the CR = 14:1 piston has a broad shallow bowl similar to the CR = 16:1 piston, rather than the narrower bowl used in most recent studies [17-20]. This CR = 14:1 piston was previously used in Ref. [21], which provides a more complete discussion of both pistons. Both pistons provide an open combustion chamber with a large squish clearance and small top-land ring crevices. Prior to running the experiments, the engine was preheated to 100°C by means of electrical heaters on the "cooling" water and lubricating-oil circulation systems. All data for this paper were taken at an engine speed of 1200 rpm. The engine specifications are listed in Table 1.

Table 1. Engine configuration used for the experiments[1]

Bore	102 mm
Stroke	120 mm
Connecting Rod Length	192 mm
Displacement	0.98 L
Compression Ratios used:	14:1, 16:1
Volume at TDC (14:1, 16:1)	75.43 cm^3 , 65.4 cm^3
Number of Valves	4
Intake Valve Opening (IVO)	0° CA
Intake Valve Closing (IVC)	202° CA
Exhaust Valve Opening (EVO)	482° CA
Exhaust Valve Closing (EVC)	8° CA
Swirl Ratio	0.7
Type of Fueling	Premixed
Engine Speed	1200 RPM
Coolant and oil temperature	~ 100 °C

[1] 0° CA corresponds to TDC intake

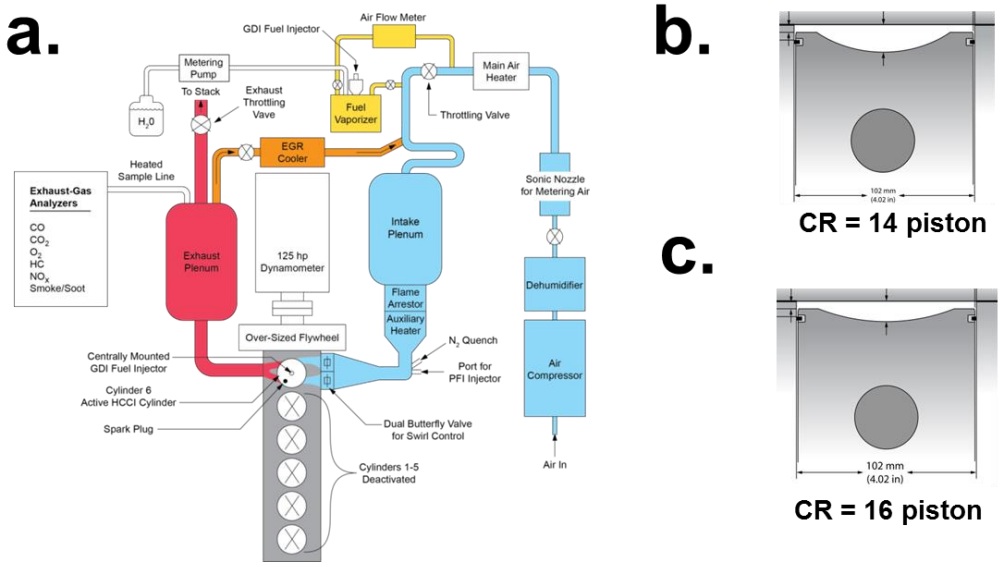

Figure 2. (a) Schematic of the LTGC (HCCI) Engine and subsystems (b) CR=14:1 piston (c) CR=16:1 piston

Air flow is supplied by an air compressor and precisely metered by a sonic nozzle as shown in Figure 2a. After the sonic nozzle, a main heater provides some preheat. A valve downstream of the sonic nozzle and main heater throttles the flow to divert a portion of the airstream through a heated and well-insulated fuel vaporizing chamber, where fuel is injected during premixed operation (see Figure 2a). The supplied amount of fuel is measured using a positive displacement flow meter and is adjusted until the desired charge-mass equivalence ratio is obtained. The vaporized fuel and air are then reintroduced with the rest of the airflow upstream of the intake plenum; a convoluted path with a series of bends ensures that the incoming charge is thoroughly mixed. The intake plenum is also well insulated and heated to a minimum of 50°C using blanket heaters to avoid fuel condensation on the plenum walls.

The insulated runner from the intake plenum to the engine is outfitted with a flame arrestor, an auxiliary heater, pressure sensors, and thermocouples. The auxiliary heater and thermocouples are mounted close to the engine to allow precise control of the T_{in}, which ranged from 60°C to 160°C for this study. For operation without EGR, the air flow was adjusted to achieve the desired intake pressure which varied from 1.0 bar (simulating naturally aspirated conditions) to 1.3 bar for the current study.

As the intake-pressure is boosted, fuel reactivity increases [15, 19], and T_{in} must be reduced to compensate. Eventually, T_{in} is reduced to 60°C, the minimum T_{in} to prevent fuel condensation in the intake system with premixed fueling. For operation with higher boost levels, T_{in} is held constant at 60°C, and cooled EGR is used to dilute the charge, reducing the autoignition propensity and allowing CA50 control. In the current study, the P_{in} = 1.6 bar data fall above this threshold, and this EGR control method was used.

After exiting the engine, the exhaust gases enter a heated plenum before being vented out the exhaust stack, as shown in Figure 2a. When EGR is used, some of the exhaust gases are recirculated back to the intake using a cooled EGR loop as also shown in the figure. With this configuration, the exhaust pressure must be greater than the intake pressure for EGR to flow into the intake system. The required back pressure is achieved by throttling the exhaust flow using the valve shown in the figure. The EGR is introduced into the intake-air upstream of the series of bends described earlier, thoroughly premixing the EGR, fuel, and air. When the valve on the EGR loop is opened, the air flow is reduced from the amount required to achieve the desired intake pressure with air alone. The exhaust back-pressure throttle valve is then adjusted to produce enough EGR flow to reach the desired intake pressure. This typically resulted in the exhaust pressure being about 2-5 kPa greater than the intake pressure. At boosted conditions, for consistency the back pressure was maintained about 5 kPa above the intake pressure, even when EGR was not used. At naturally aspirated conditions the exhaust back pressure was left unthrottled. The flow rate of the cooling water for the EGR loop can be adjusted to control the temperature of the EGR gases to temperatures as low as 30°C. A water trap downstream of the EGR cooler removes the water that condenses if the EGR gases are cooled below their dew point.

Modified Cylinder Head and Spark Plug Details

A new spark-plug capable cylinder head was obtained to perform the experiments in this paper. For SA work, ideally the spark plug would be centrally mounted to maximize the active flame area and minimize heat transfer losses that may occur due to flame-wall interactions. However, since some of our current and future work includes DI fueling, and adequate mixing with minimal wall wetting is important, an imposed design constraint was that the GDI injector remain in the center

of the combustion chamber. Selecting an alternative location for the spark plug was nontrivial due to potential interference with water cooling channels and oil passageways and the valves. With the chosen design, a port for a spark plug with 10 mm diameter threads was added 42 mm off-center, which is approximately the same location where the water cooled pressure sensor was mounted in previous studies (AVL QC33C or QC34C) [19, 11, 16]. To avoid any interference with the aforementioned cooling channels, a smaller 5 mm diameter pressure sensor was used (AVL GH15D) with access to the cylinder via a horizontal port through the firedeck and connected to the combustion chamber with a short conical passage.

Figure 3 shows a cross-sectional view of the cylinder head and spark-plug port, which is inclined at an angle of 27.2° from vertical. The spark-gap protrudes about 2 mm below the firedeck surface. Figure 4 shows the position of the spark plug electrode relative to the centrally mounted GDI injector, horizontal pressure transducer port, and the intake and exhaust valves.

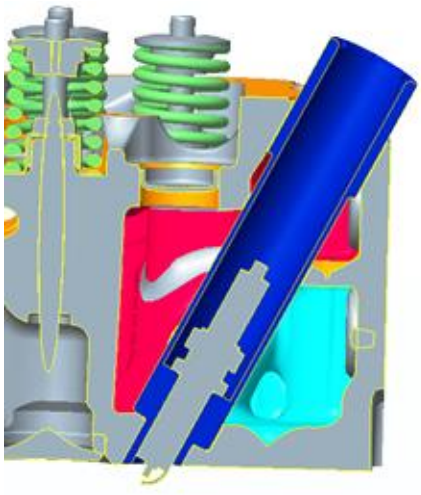

Figure 3. Cross-sectional view of the cylinder head showing the installation of the spark plug.

The ignition coil used was a coil-on-plug conventional inductive ignition system built by Diamond Electric. The charge build-up duration was set to 3.2 ms, which provided the maximum amount of ignition energy, 93 mJ. To ensure that breakdown was occurring, a current probe was used around the ignition coil ground cable to monitor the secondary current profile up to TDC for motored operation at each operating condition. As the intake pressure was increased, the spark-plug gap was reduced to keep the required breakdown voltage from becoming too high, in order to prevent intermittent misfires from a failed spark breakdown that might damage the spark plug or ignition system. The electrode gap sizes used for the different intake pressures are summarized in Table 2.

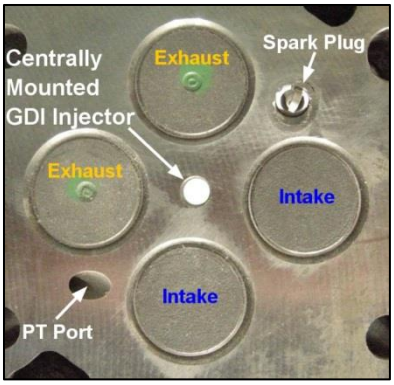

Figure 4. View of the cylinder head showing the centrally mounted GDI fuel injector, and the relative locations of the intake and exhaust valves, horizontal pressure transducer port, and spark plug.

Table 2. Spark plug details and gap sizes used

Spark Plug	10 mm NGK DFE Iridium
Spark Plug Gap size (mm)	
CR=16:1, P_{in}= 1.0 bar	0.787 mm
CR=14:1, P_{in}= 1.0 to 1.3 bar	0.610 mm
CR=14:1, P_{in}= 1.6 bar	0.508 mm
Ignition Coil	Conventional Induction
Charge Buildup duration	3.2 ms
Ignition Energy	93 mJ

Fuel Specifications

Two different fuels were tested with properties representative of premium- and regular-grade market gasolines. The first fuel was a standard Tier II certification gasoline supplied by Haltermann Solutions with an AKI = 92.2 (RON 96.0), which is comparable to premium-grade gasolines with zero ethanol content; It will be referred to as CF-E0 (certification fuel, zero ethanol). The second fuel was a research-quality, regular-grade E10 gasoline named RD5-87. This fuel was designed to be representative of current regular-grade E10 fuels sold in the U.S., and has been used in several of our previous publications [17]. However, during the current work, a new batch of RD5-87 was used and appeared to be more reactive than previous batches. A detailed hydrocarbon analysis (DHA) along with RON and MON testing performed by Southwest Research Institute confirmed this, with the results listed in Table 3. The letters “a” and “b” are used to differentiate between the old and new batches, respectively. Despite the compositional differences between “a” and “b”, the heating values are comparable.

Table 3. Fuel properties for CF-E0 and RD5-87

	CF-E0	RD5-87a	RD5-87b
Net Heat of Combustion [MJ/kg]	43.296	41.639	41.642
RON — ASTM D2699	96.0	92	90.6
MON — ASTM D2700	88.3	84.9	83.9
Antiknock Index (AKI)	92.2	88.5	87.3
Sensitivity = Ron – Mon	7.7	7.1	6.7
Hydrocarbon Type [vol %]			
Paraffins	7.715	16.868	16.684
I-Paraffins	49.272	31.76	32.012
Aromatics	37.449	22.122	22.806
Napthenes	3.076	11.447	12.147
Olefins	6.551	6.511	5.941
Oxygenates	0.0	9.97	10.58
Carbon [wt %]	86.62	82.26	82.28
Hydrogen [wt %]	13.57	13.98	13.80
Oxygen [wt %]	0.0	3.67	3.89
A/F Stoichiometric	14.54	14.06	13.98

Data Acquisition

The pressure transducer signals from the horizontally mounted AVL GH15D sensor were digitized and recorded at ¼° CA increments for one hundred consecutive cycles. The cylinder-pressure transducer was pegged to the intake pressure near bottom dead center (BDC) where the cylinder pressure reading was virtually constant for several degrees. For all data presented, 0° crank angle (CA) is defined as TDC intake (so TDC compression is at 360°). This eliminates the need to use negative crank angles or combined bTDC, aTDC notation.

The crank angle of the 50% burn point (CA50) was used to monitor the combustion phasing. CA50 was determined from the cumulative apparent heat-release rate (AHRR), computed from the cylinder-pressure data (after applying a 2.5 kHz low-pass filter [21]. Computations were performed for each individual cycle, disregarding heat transfer and assuming a constant ratio of specific heats [22].[2] The average of 100 consecutive individual-cycle CA50 values were then used to monitor CA50 during engine operation and for the values reported. The reported ringing intensities are computed from the same low-pass-filtered pressure data.

LTGC/HCCI combustion is often limited by high peak-pressure-rise-rates (PPRRs), which cause acoustic oscillations in the charge gas resulting in audible engine knock. If this phenomenon is not controlled, it can result in unacceptable noise levels and potentially, engine damage. The acceptable knock limit for LTGC engines is often defined in terms of a maximum allowable PRR ($dP/d\theta$, where θ is a variable representing °CA). However, this does not correctly reflect the potential for knock with changes in intake boost or engine speed. In this work, the correlation for ringing intensity (RI) developed by Eng [23] is used as a measure of the propensity for engine knock.

$$RI = \frac{1}{2\gamma} \cdot \frac{\left(0.05 \cdot \left(\frac{dP}{dt}\right)_{max}\right)^2}{P_{max}} \cdot \sqrt{\gamma R T_{max}} \qquad (2)$$

Where $(dP/dt)_{max}$, P_{max}, and T_{max} are the maximum values of PRR in real time (i.e. the PPRR), pressure, and temperature, respectively γ is the ratio of specific heats (c_p/c_v), R is the gas constant, and 0.05 is an empirical correlation constant introduced by Eng which has units of milliseconds. The ringing is a measure of the acoustic energy of the resonating pressure wave that creates the sharp sound commonly known as engine knock. Based on the onset of an audible knocking sound and the appearance of strong ripples on the pressure trace, a ringing criterion of RI = 5 MW/m^2 was selected as the ringing limit for operation without knock. This is the same limit used in our previous works, for example [17, 18] and a more complete discussion of the selection of this value may be found in Ref.[20] This value, 5 MW/m^2, corresponds to about 8 bar/°CA at 1200 rpm, naturally aspirated. However, it should be noted that the allowable PPRR increases with boost due to the increased value of P_{max} in the denominator of Eq. 2. At all boost levels tested, audible engine knock correlated well with the RI rising above 5 MW/m^2, giving confidence in this correlation.

Exhaust emissions data were also acquired, with the sample being drawn from the exhaust plenum using a heated sample line (see Figure 2). CO, CO_2, HC, NOx, and O_2 levels were measured using standard exhaust-gas analysis equipment. In addition, a second CO_2 meter monitored the intake gases just prior to induction into the engine. For tests with EGR, this allowed the EGR fraction to be computed from the ratio of the intake and exhaust CO_2 concentrations.

Results and Discussion

Demonstration and Initial Investigation of SA-LTGC

The first set of experiments was performed with CR=16:1, using CF-E0 as the fuel, at naturally aspirated intake conditions (P_{in}=1.0 bar), and with ϕ_m = 0.42. To illustrate the effect of the spark and the subsequent flame propagation with SA, in-cylinder pressure traces and heat release rates are shown in Figure 5a. Figure 5b gives a close-up view of these initial heat release rates. In both figures, the black curves correspond to CI-only, at an intake temperature that gave RI=5 MW/m^2. For the SA curves, the spark timing is indicated by a dashed line punctuated by a lightning-bolt symbol to represent the deposition of the electrical energy.

[2] This specific heat ratio (γ) is determined from a fit to the actual pressure data to account for differences in gas temperature or EGR levels between operating conditions. Comparison of CA50 values computed in this manner with those computed by detailed calculations using real-gas properties that vary over the cycle and a Woschni heat transfer corrections shows good agreement, with differences typically being less than one or two tenths of a degree.

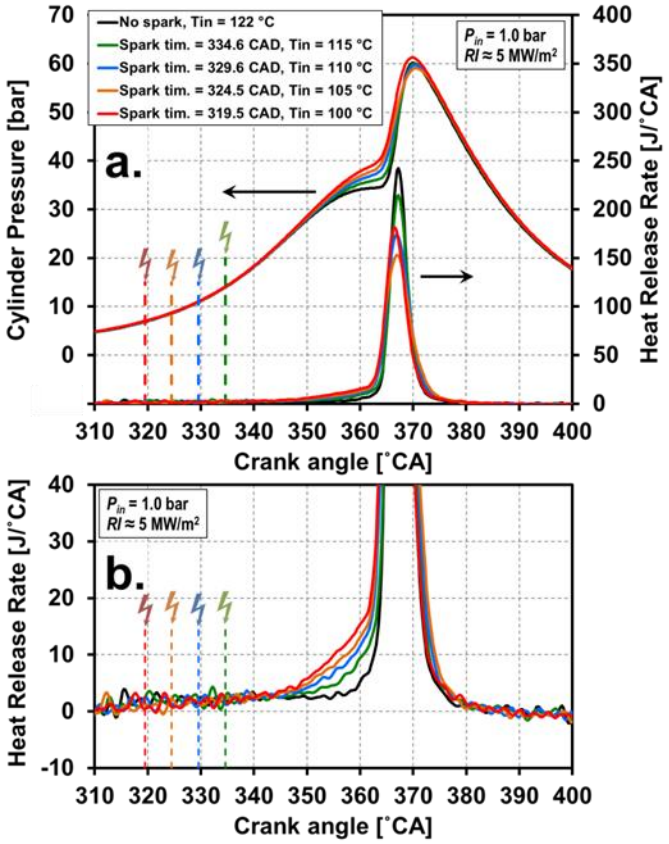

Figure 5. CR=16:1, CF-E0, P_{in}=1.0 bar: (a) Cylinder pressures and heat release rates for CI and SA (b) Close-up view of the early heat release rates.

With SA, as the intake temperature is decreased, the spark has to be advanced to maintain RI=5 MW/m^2. This is necessary because the autoignition reactivity diminishes as T_{in} is decreased, so more compression heating from the expanding flame front is required. Advancing the spark gives more time for flame propagation, and therefore, more flame-induced compression of the remaining charge. Additionally, the laminar flame speed decreases with both reduced T_{in} and with earlier spark timing (due to lower in-cylinder temperatures), further increasing the spark advance required. For this reason there is less charge-mass remaining at the time of autoignition, which reduces the peak cylinder pressures and peak heat release rates, which occur when the majority of the charge burns by CI. Referring back to figure 5a, the data follow this trend well with the exception of the T_{in}=100°C (red) curve, which has the highest peak cylinder pressure and a peak heat release rate comparable to T_{in} = 130°C. This anomalous behavior is thought to be due to the slightly advanced CA50 and marginally higher ringing intensity of this data point compared to the others. Nevertheless, it can be seen that the first part of the heat release associated with flame propagation increases as intake temperature decreases and it contributes a significant fraction of the total, up to about 15% for the conditions presented here.

SA and CI-only are further compared in Figure 6 by considering the allowable ranges of T_{in} for both methods. For CI only, T_{in} was cooled from 122°C, which gives RI=5 MW/m^2, down to 118°C, at which point CA50 becomes so retarded that combustion stability increases to a COV-IMEP$_g$=2%. This is shown in Figure 6a by the red curve with open data markers, where T_{in} is along the abscissa and COV-IMEP$_g$ is along the secondary ordinate. Also, as T_{in} was reduced and CA50 became more retarded, the ringing intensity decreased as shown in Figure 6b (open data markers indicate CI only).

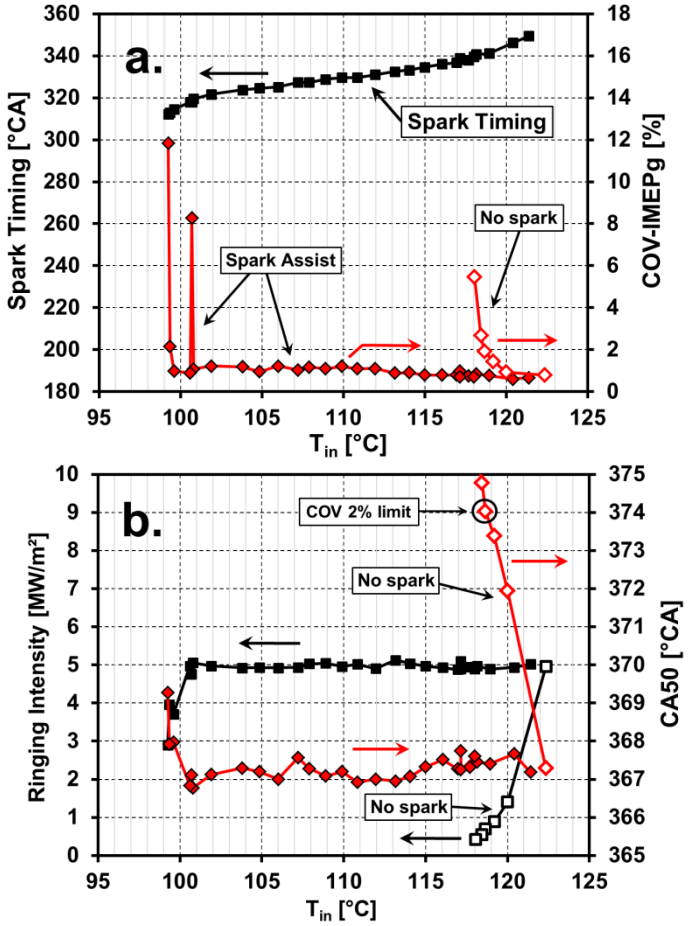

Figure 6. CR=16:1, CF-E0, Pin=1.0 bar: (a) Tin vs spark timing, COV-IMEPg, (b) Tin vs RI, CA50.

For the SA sweep, the initial T_{in} was just a little below that required to obtain RI=5 MW/m^2 for CI only, and the spark timing was adjusted to obtain RI=5 MW/m^2 with this lower temperature. Then, as T_{in} was further decreased over the sweep, the spark timing was progressively advanced to maintain a constant ringing intensity. This resulted in the COV-IMEP$_g$ and the combustion phasing being nearly constant for most of the sweep as seen in Figure 6a and Figure 6b, respectively. The intake temperature was able to be decreased until T_{in}=100 °C, when the COV-IMEP$_g$ rapidly increased well beyond 2%. Importantly, this intake temperature is significantly colder compared to when the combustion stability started to deteriorate with CI only, with ΔT_{in}=22°C for SA from RI=5 MW/m^2 to COV-IMEPg = 2%, instead of ΔT_{in}=4°C for CI only.

Next the amount of CA50 control authority was investigated for two selected intake temperatures, as shown in Figure 7. For this figure it is convenient to now present the same T_{in} and spark timing data shown in Fig. 6a with the axes switched—with the spark timing now as the abscissa and T_{in} along the

primary ordinate. For the two CA50 control sweeps, the data markers are circled to indicate the intake temperatures and spark timings that gave RI=5 MW/m^2. The first CA50 control sweep at T_{in}=117°C corresponds to the T_{in} that gives a limiting, unstable CI-only condition (COV-IMEP$_g$=5%), while the second sweep was taken at a temperature 10°C lower (107°C), where combustion would not occur if the spark was turned off. For both control sweeps, the intake temperature was held constant while varying the spark timing to advance CA50 to the onset of knocking (RI=5 MW/m^2) and then retarding CA50 until combustion became unstable (COV-IMEP$_g$>2%). These limits are connected by dashed lines, with the stability limits identified by starred data points. The sweeps show that SA can provide about 6.5° CA of CA50 control at T_{in}=117°C, while at T_{in}=107°C only 2.3° CA of CA50 control is possible.

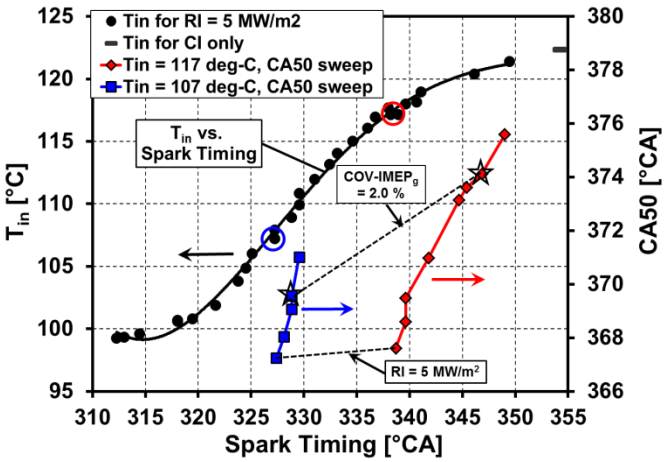

Figure 7. CR=16:1, Pin=1.0 bar, using CF-E0. CA50 Control sweeps at two selected intake temperatures.

Effects of Changing Fuel and CR

Figure 8 shows the effects of changing the fuel and compression ratio by considering the T_{in} and spark timing relationships to obtain RI=5 MW/m^2 at ϕ=0.42. Horizontal dashed lines in this figure give a baseline by showing the intake temperatures needed for CI-only with RI = 5 MW/m^2. The black curve is the same data shown previously in Figure 6 and Figure 7 for CR=16:1 using CF-E0. Keeping the CR at 16:1 and changing the fuel to RD5-87[3] requires that lower T_{in}s be used, due to the higher autoignition propensity for RD5-87. However, when the CR is reduced to 14:1, RD5-87 requires higher T_{in}s than CF-E0 with CR=16:1. Also, for RD5-87 with CR = 14:1, earlier spark timings are required to maintain RI=5 MW/m^2 than for CF-E0 with CR=16:1.

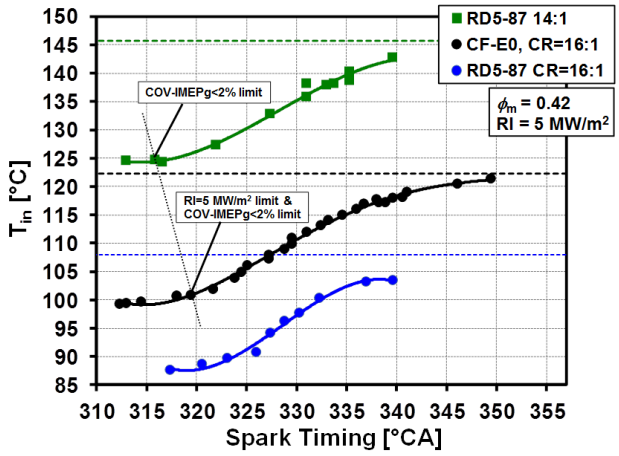

Figure 8. Effects of compression ratio (CR=16:1, 14:1) and Fuel (CF-E0, RD5-87) on intake temperature and spark timing. Horizontal dashed lines indicate the intake temperature required for RI=5MW/m^2 for CI-only.

Furthermore, it should be noted that with CR=16:1 and CF-E0, with the proper spark timing, the T_{in} with SA is shown to closely approach the T_{in} for CI-only. For the other curves, since the points near the CI baseline are stable and can be easily obtained by extrapolation, the spark timing data wasn't collected close to the CI-only baseline. Instead, the start of the sweep was defined by lowering the intake temperature until RI=3 MW/m^2 with CI-only, then turning the spark on and adjusting the timing to bring the ringing intensity back to RI=5 MW/m^2. This results in a small gap between the curves and the Tin for the CI-only baseline caused only because data were not collected in this region; it should not be misinterpreted as a limit to the sweep. The COV-IMEP$_g$ limits to the sweeps at the lower Tins were determined by the last data points where the COV-IMEP$_g$ < 2%, as indicated by a dashed line in Figure 8. For the CF-E0 curve, the ringing intensity also fell below 5 MW/m^2 at this point, but it was still possible to stabilize the combustion at a lower ringing intensity until the COV-IMEP$_g$ suddenly increased again (see Figure 6). A limit isn't shown for the CR=16:1 RD5-87 curve because the COV-IMEP$_g$ data was thought to be unreliable due to the pressure sensor starting to fail, but the general trend in T_{in} and spark timing is expected to be correct.

Detailed Investigation of SA-LTGC at Naturally Aspirated Conditions

Studies at a base condition with ϕ_m=0.42

Figure 9 shows the intake temperature and spark timing sweep at ϕ=0.42, for CR=14:1 and RD5-87 (replotted from Figure 8), along with plots of the RI and COV-IMEP$_g$ for this sweep. For the remainder of the paper, all of the results will be using this fuel and compression ratio. The T_{in} required for CI-only with RI = 5 MW/m^2 is shown by a horizontal bar on the right hand side of the plot. Similar to the CR=16:1 results using CF-E0 in Figure 6, the ringing intensity and COV-IMEP$_g$ could be held nearly constant while decreasing T_{in} and advancing the spark timing until a rapid increase in COV-IMEP$_g$ beyond 2%. The maximum amount that T_{in} could be decreased, from the CI-only point with RI=5 MW/m^2 until COV-IMEP$_g$ >2 with SA, was

[3] As discussed in the experimental methods RD5-87 had different properties depending on the batch used. The CR= 16:1 curve in Figure 8 is the only data presented for RD5-87a, while the rest of the data in the paper are for RD5-87b.

ΔT_{in}=21°C. Notably, this is almost identical to the ΔT_{in}=22°C obtained earlier with CR=16:1 using CF-E0.

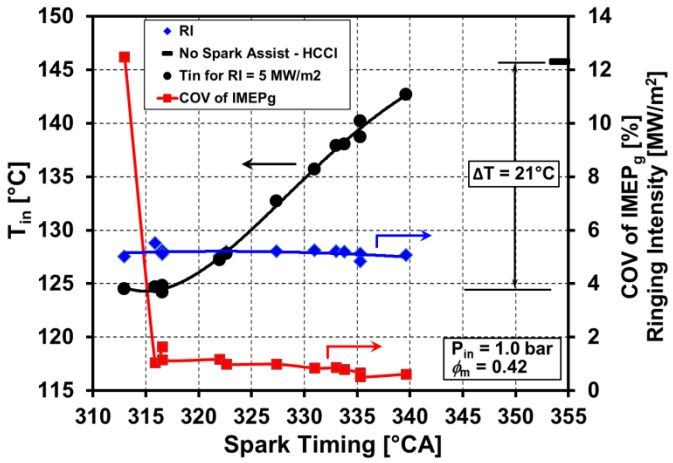

Figure 9. Intake temperature and spark timing for CR=14:1 using RD5-87 at P_{in}=1.0 bar.

To investigate the combustion behavior and to determine what causes the COV-IMEP$_g$ to increase so rapidly at the low T_{in} limit for SA, the data presented in Figure 9 were replotted in Figure 10 with T_{in} as the abscissa, very similar to how the data was shown previously in Figure 6. This allows the CI-only and SA curves to be plotted along a common axis and facilitates a comparison between the two sweeps. Points of interest were identified, and at these points, the heat release rates (HRR) are plotted in Figure 11. In this figure, each sub-plot corresponds to a point of interest as denoted by the data points labeled 1 – 5 in Figure 10, and the grey curves show the HRR of each of the 100 individual cycles acquired and the red curve shows the cycle-averaged HRR. For CI-only with RI=5 MW/m^2 (point 1), the grouping of the individual-cycle HRRs is relatively tight with little variability (COV-IMEP$_g$=0.70%). However, when T_{in} is decreased to T_{in}=139°C (point 2), the peak HRRs are significantly lower and the combustion phasing shows greater variability; these attributes cause the cycle-averaged curves to exhibit RI=0.95 MW/m^2 and COV-IMEP$_g$=2%. When the spark plug is turned on at nominally the same intake temperature (T_{in}=140°C) (point 3), and the spark timing is adjusted to give RI=5 MW/m^2, compression heating from the flame advances CA50, increases the peak pressure, and reduces the cycle-to-cycle variability of the HRR for a COV-IMEP$_g$=0.87%, which is comparable to the CI-only case at T_{in}=145°C. When T_{in} is decreased further to T_{in}=127°C (point 4), there appears to be more variability in the heat release and combustion phasing, but this only marginally increases the mean COV-IMEP$_g$ to 1.28%, which is still an acceptable value. However, reducing T_{in} slightly to 124°C and advancing the spark timing to 312° CA (point 5) results in a rapid increase in COV-IMEP$_g$ as evident in Figure 10. Figure 11 shows that this increase in COV-IMEP$_g$ is due to a few complete misfire cycles, as indicated by the blue HRR curves. Excluding the misfire cycles, the overall variability is similar to the curves presented for point 4, when T_{in}=127°C and the spark timing = 316° CA. As discussed in the introduction, Persson et al. also attributed the rapid rise in COV-IMEP$_g$ that they observed to misfire cycles when their spark timing was advanced to 305° CA.

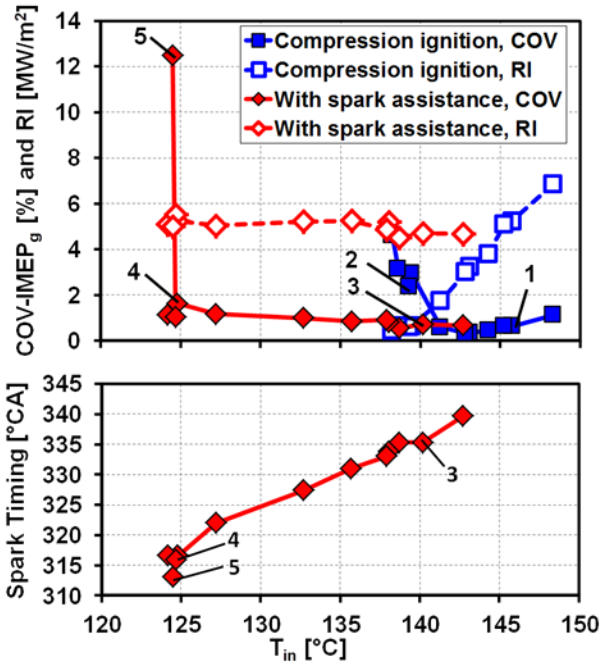

Figure 10. Ringing Intensity and COV-IMEP$_g$ for CI and SA. The numbered data points correspond to the numbered sub-plots in Figure 11. CR=14:1, Pin=1.0 bar, using RD5-87.

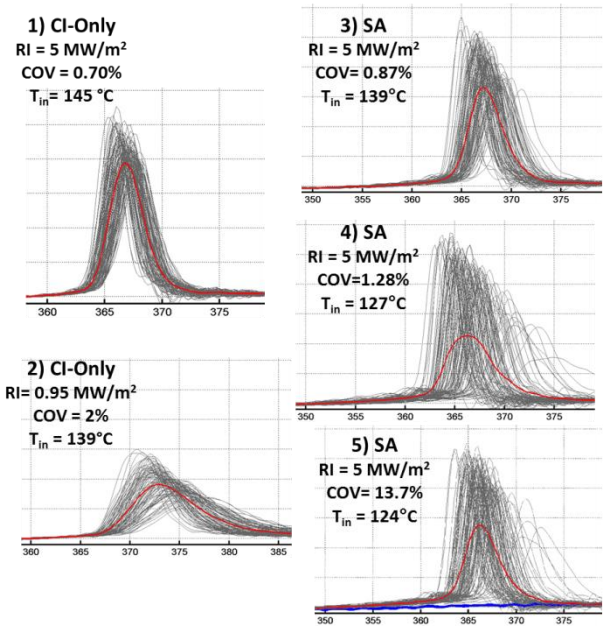

Figure 11. Individual cycle and cycle-averaged heat release rates. The numbers of the sub-plots correspond to the data points labeled in Figure 10. CR=14:1, Pin=1.0 bar, using RD5-87.

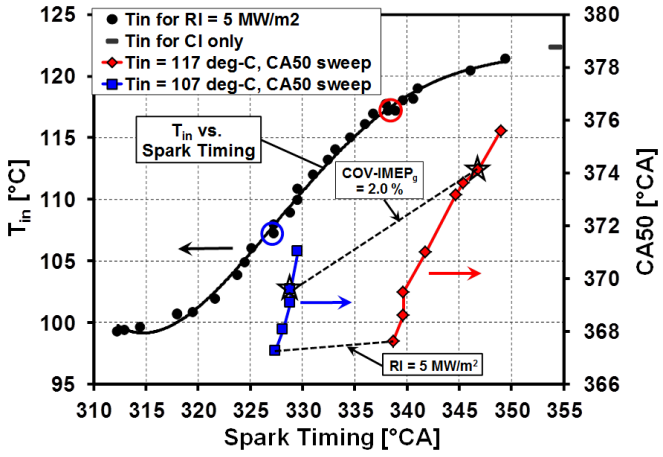

Figure 12. CA50 Control sweeps for CR=14:1 using RD5-87.

Figure 12 presents two CA50 control sweeps at CR=14:1 using RD5-87, analogous to the sweeps performed in Figure 7 for CF-E0 and CR=16:1. However, here the sweeps were extended past the onset of knocking (RI=5 MW/m^2) to the point where RI=7 MW/m^2 (heavy knocking), to show that SA could still be used as an effective means of control under these conditions. For the various sweeps performed in Figures 7 and 12, the amount of control authority is summarized in Table 4.

Table 4. Summary of CA50 control authority for selected conditions at P_{in}=1.0 bar and ϕ_m=0.42

	T_{in} for COV-IMEP$_g$=5% with CI-Only	T_{in} =10°C lower than for COV-IMEP$_g$=5% with CI-Only
CR=16:1,CF-E0, P_{in}=1.0 bar:	**T_{in}= 117°C**	**T_{in}= 107°C**
RI=5 MW/m^2 to COV-IMEP$_g$=2%	ΔCA50= 6.5° CA	ΔCA50= 2.3° CA
CR=14:1, RD5-87, P_{in}=1.0 bar:	**T_{in}= 138°C**	**T_{in}= 128°C**
RI=7 MW/m^2 to COV-IMEP$_g$=2%	ΔCA50= 7.0° CA	ΔCA50= 4.6° CA
RI=5 MW/m^2 to COV-IMEP$_g$=2%	ΔCA50= 5.4° CA	ΔCA50= 3.0° CA

For analogous T_{in}'s corresponding to COV-IMEP$_g$ = 5% with CI-only, the maximum ΔCA50 at CR=14:1 using RD5-87 is 5.4° CA, about 1° CA less than what could be achieved at CR=16:1 using CF-E0. However, using CR=14:1 and RD5-87 provides slightly more control when the T_{in} is lowered 10°C, with 3.0° CA of control, compared to 2.3° CA using CR=16:1 and CF-E0.

It is important to note that for the sweeps performed at the different intake temperature and for a given CR, the amount of CA50 control is determined by the obtainable CA50 at the RI limit and the COV-IMEP$_g$ = 2% limit; however, for these conditions the combustion phasing for RI=5 MW/m^2 or RI=7 MW/m^2 occurs at nearly the same CA50, regardless of the T_{in} that the sweep was performed at. The COV-IMEPg = 2% limit results from having too little time for the flame to propagate to provide enough compression to autoignite the main charge.

For the T_{in}'s that yield COV-IMEP$_g$=5% with CI-only (T_{in}=117°C and T_{in}=138°C, for CR= 16:1 and CR=14:1, respectively), retarding the spark beyond the values shown will cause the COV-IMEP$_g$ to increase further until it reaches this baseline COV-IMEP$_g$ value for CI-only. However, for the CA50 control curves that were performed 10°C lower, the temperature is too low to produce autoignition with CI-only, so retarding the spark timing will eventually result in a misfire as the flame propagation time becomes too short to provide sufficient compression for autoignition.

Effects of equivalence ratio on allowable ΔT_{in} and required spark timing at P_{in} = 1 bar

T_{in} and spark timing curves for four selected equivalence ratios are shown in Figure 13a. As in Figure 12, horizontal bars near the right hand side of the plot represent the T_{in}s required for CI-only at RI=5 MW/m^2. The ϕ_m=0.42 curve is the same base-condition data shown previously in Figures 9-12. As the equivalence ratio is increased to ϕ_m=0.45, the baseline T_{in} for CI-only has to be decreased to compensate for higher wall and residual gas temperatures. Conversely, at the lower equivalence ratios of ϕ_m=0.38 and ϕ_m=0.36, more intake heating is required. Similar to the results presented earlier, for ϕ_m=0.42 and ϕ_m=0.45 the ringing intensity could be held at RI=5 MW/m^2 while decreasing T_{in} and advancing the spark timing to compensate until COV-IMEP$_g$>2%. The dashed line on the figure indicates this limit. However, as T_{in} was reduced for ϕ_m=0.38 and ϕ_m=0.36 the sweeps did not become stability limited, i.e. the COV-IMEP$_g$ remained < 2%. Instead the low-T_{in} end of these sweeps was determined by the point where the ringing intensity could not be maintained at RI=5 MW/m^2 due to the reduced compression heating from the weak flame propagation. Figure 13b summarizes the allowable T_{in} reduction for these equivalence ratios, with the limits determined by COV-IMEP$_g$>2% (ϕ_m= 0.42 and 0.45) or RI<5 MW/m^2 (ϕ_m= 0.38 and 0.36).

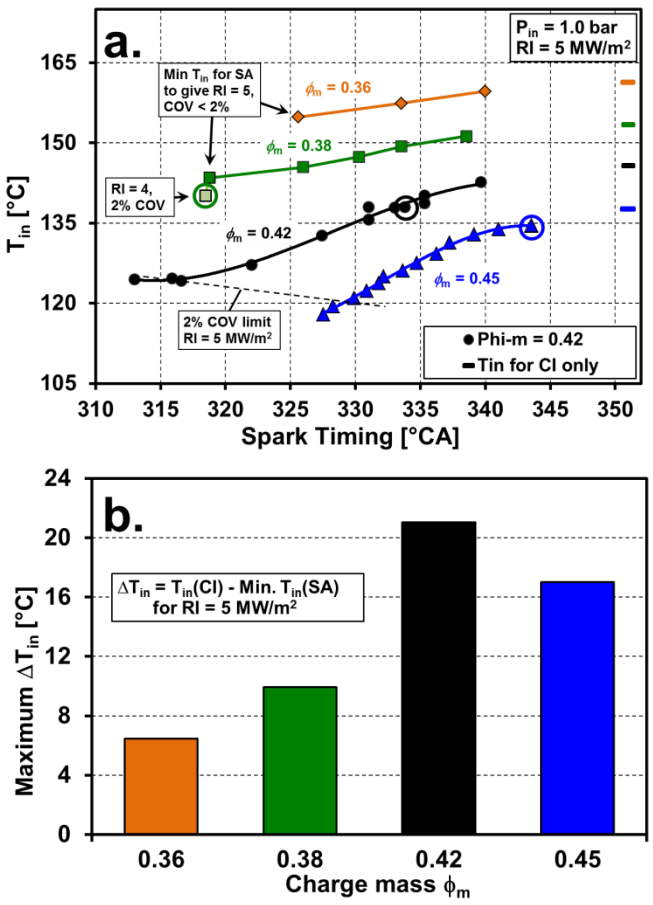

Figure 13. Effects of Equivalence ratio: (a) T_{in} vs spark timing sweeps (b) Summary of allowable intake temperatures.

Based on these findings at P_{in}=1.0 bar, ϕ=0.42 appears to be near the optimal value to obtain the maximum allowable ΔT_{in}. At equivalence ratios higher than ϕ_m=0.42, the autoignition becomes inherently more unstable as the knock-stability limit narrows [24]. Furthermore, although a higher equivalence ratio enhances the flame propagation, the ratio of specific heats for the mixture is reduced, which causes the unburned mixture to experience less compression from the propagating flame. Conversely, equivalence ratios lower than ϕ_m=0.42 experience more effective compression from the increased ratio of specific heats, but less compression actually occurs because the flame propagation rate is slower, resulting in RI<5 MW/m^2.

Effects of equivalence ratio on CA50 control at P_{in}=1.0 bar

The effects of equivalence ratio on the ability to provide CA50 control with SA are shown in Figure 14. The control sweep with SA from Figure 12 at ϕ_m=0.42 for a T_{in} corresponding to COV-IMEP$_g$ = 5% for CI-only is replotted here. The ϕ_m=0.38 sweep was also performed at an analogous T_{in}. However, at ϕ=0.45, operating at this point is challenging due to the convergence of the knock and stability limits, so the T_{in} corresponding to CI-only with COV-IMEP$_g$=3% was used instead.

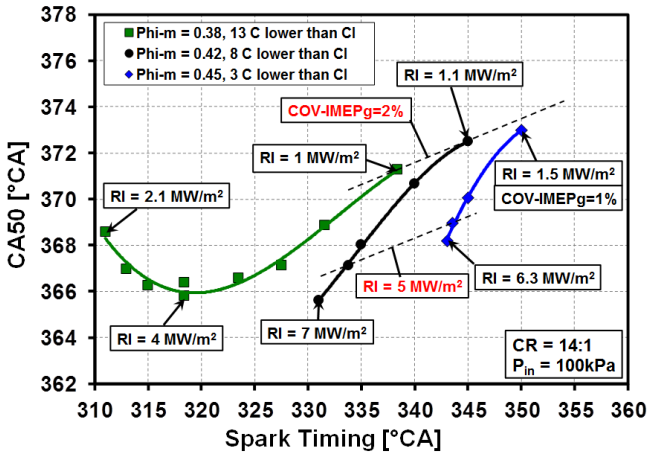

Figure 14. Effects of Equivalence ratio on CA50 control authority at selected conditions.

Using SA with ϕ_m=0.38, the RI did not increase beyond 4 MW/m^2, but the CA50 could still be advanced, up to about 366°CA, with a spark timing occurring at 318.4°CA. For ϕ_m=0.42, the spark timing could be advanced to 334°CA until RI = 5 MW/m^2, or even further to 331°CA with RI= 7 MW/m^2, while still maintaining control. When the equivalence ratio was increased to ϕ_m=0.45, a more retarded CA50=368.5 °CA was required for RI = 5 MW/m^2, which required later spark timings so that less compression heating from the flame occurred. This is in contrast to the control sweeps performed at different temperatures at a constant CR and ϕ_m, where the CA50 corresponding to the RI=5 MW/m^2 limit was nearly constant. Thus, one effect of increasing the equivalence ratio on CA50 control is that the allowable CA50 at the RI = 5 MW/m^2 limit has to be more retarded to prevent ringing, thus requiring later spark timings. However, it is noteworthy that increased CA50 retard with increased ϕ_m is much larger than the required increase in spark-timing retard, probably because of the higher flame speeds with higher ϕ_m. The COV-IMEP$_g$=2% limit was discussed previously, and the effect of increasing equivalence ratio on this limit is that the CA50 can occur later in the cycle before this limit is reached; however, later spark timings are also required to achieve this. Table 5 summarizes the amount of CA50 control authority for these sweeps.

Table 5. Summary of CA50 control authority for the sweeps performed in Figure 14.

RD5-87 CR=14:1 P_{in}=1.0 bar	ϕ_m	T_{in}	ST for most advanced CA50	Most advanced CA50	ST at COV-IMEPg=2%	CA50 at COV-IMEPg=2%	ΔST	ΔCA50
RI=4 MW/m^2 to COV-IMEPg=2%	0.38	142°C	318.4° CA	365.8° CA	338.4° CA	371.3° CA	19.9° CA	5.5° CA
RI=5 MW/m^2 to COV-IMEPg=2%	0.42	138°C	333.8° CA	367.1° CA	345.0° CA	372.5° CA	11.2° CA	5.4° CA
RI=7 MW/m^2 to COV-IMEPg=2%	0.42	138°C	331.0° CA	365.7° CA	345.0° CA	372.5° CA	14.0° CA	6.9° CA
RI=5 MW/m^2 to COV-IMEPg=2%	0.45	134°C	343.6° CA	369.0° CA	352.0° CA	374.1° CA	8.4° CA	5.2° CA

Effects of increasing Intake Pressure

Figure 15 shows the effect of increasing intake-boost pressure on spark timing and T_{in} for P_{in}s up to 1.3 bar. On the right hand side of this plot, data markers show the combustion phasing and T_{in} for CI-only. As intake pressure increases, the fuel becomes more reactive and the T_{in} needs to be lower to maintain RI=5 MW/m^2. It can also be seen that the combustion phasing for CI-only has to be more retarded to maintain the ringing intensity since the greater charge density leads to faster pressure rise rates.

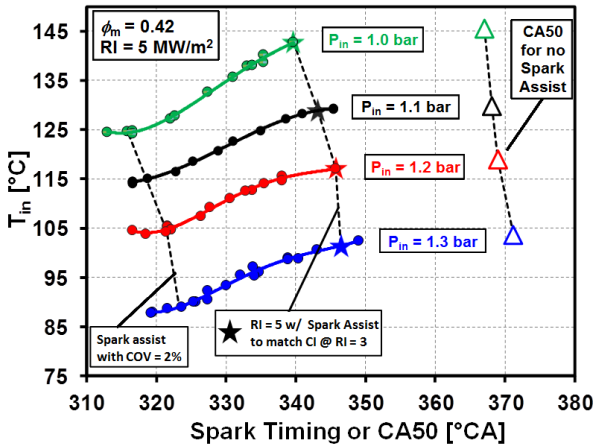

Figure 15. Effects of intake pressure boost on T_{in} and spark timing (P_{in}=1.0 to 1.3 bar).

When the intake pressure was increased to P_{in}=1.6 bar, the fuel reactivity increased further, and dropping T_{in} to 60°C was insufficient to keep RI from exceeding 5 MW/m^2, so cooled external EGR was added to dilute the mixture[4]. As described in the introduction, increasing the amount of EGR decreases the oxygen concentration, which decreases global reactivity in a manner similar to decreasing the intake temperature. Thus, similar to the sweeps performed by dropping T_{in}, lower oxygen concentrations (higher EGR levels) can be tolerated with SA than with CI alone. Figure 16 shows an EGR and spark timing sweep for P_{in} = 1.6 bar, analogous to the sweeps in Figure 15.

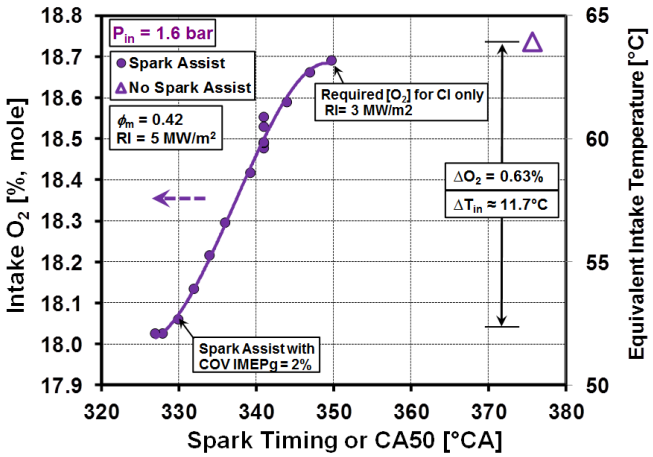

Figure 16. Effects of oxygen concentration (EGR level) on the spark timing required to maintain RI=5 MW/m^2 for an intake-pressure of 1.6 bar, the right-hand axis shows the equivalent change in T_{in} based on the study in the Appendix.

[4] T_{in}=60°C is the coolest intake temperature that can be used with premixed operation before fuel starts to condense in the intake system.

The allowable decrease in oxygen concentration from RI=5 MW/m^2 to COV-IMEP$_g$=2% was found to be ΔO_2=0.7%. An experiment described in the appendix was performed to relate this decrease in oxygen concentration to a comparable ΔT_{in}; using these results ΔO_2=0.7% was estimated to be equivalent to approximately ΔT_{in}=12°C. Using this ΔO_2-to-ΔT_{in} conversion to provide a common scale allows the sweeps for all the different intake pressures to be shown on the same plot in Figure 17a. In this figure, the COV-IMEP$_g$=2% limits are indicated by stars with an unfilled center, while the filled stars show the SA RI=5 MW/m^2 point at the T_{in} that gives RI=3 MWm^2 for CI-only.

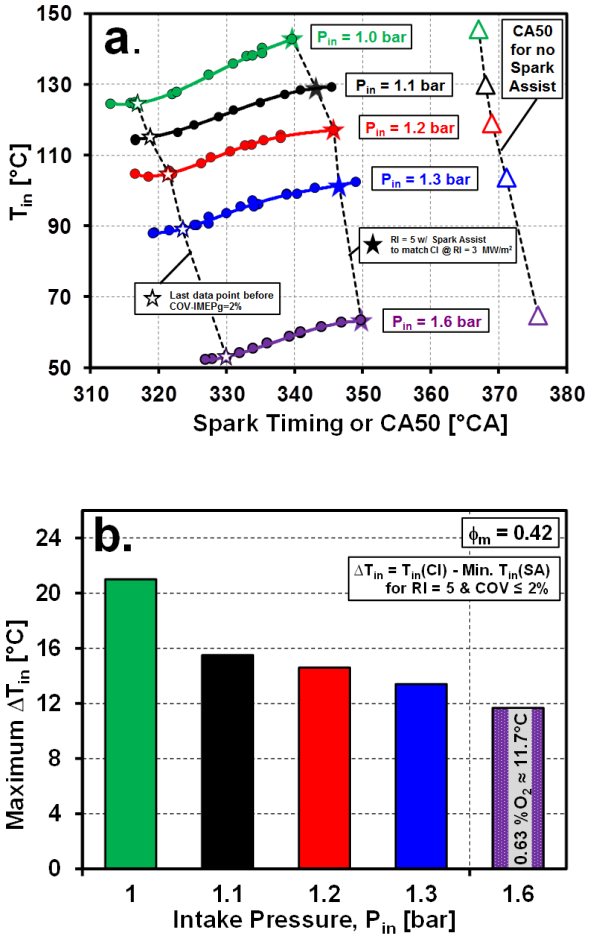

Figure 17. Effects of Intake pressure boost, with P_{in}=1.6 bar plotted using an equivalent ΔT_{in} (a) spark timing and intake temperature sweeps (b) summary of maximum allowable ΔT_{in} with intake-pressure boost.

Recall that earlier (first defined for Figure 9) the maximum allowable ΔT_{in} was defined as the difference between the intake temperature obtained with CI at RI=5 MW/m^2 and the lowest allowable temperature before COV-IMEP$_g$ > 2%. This maximum allowable ΔT_{in} decreases with intake pressure, as evident from the bar graph in Figure 17b. The largest decrease in ΔT_{in} occurs as P_{in} is increased from 1.0 to 1.1 bar, and then, it decreases more moderately with intake pressure. At P_{in}=1.0 bar, ΔT_{in}=21°C, while increasing the boost pressure to P_{in}=1.6 bar decreases the range to ΔT_{in}=12°C.

A CA50 control sweep at P_{in}=1.6 bar is shown in Figure 18. For this sweep, the intake oxygen concentration was held constant at a value that gave COV-IMEP$_g$=5% with CI-only (analogous to the higher-temperature control sweep at P_{in}=1.0 bar). To demonstrate the full control range, the limits were defined from RI=7 MW/m^2 to COV-IMEP$_g$ =3%, which resulted in 5.1° CA of CA50 control. However, to compare with the sweeps taken at P_{in}=1.0 bar, consistent limits from RI=5 MW/m^2 to COV-IMEP$_g$=2% should be used, which are also shown on the figure. Between these limits only 3.2 °CA of control was possible at P_{in}=1.6 bar compared to 6.5 °CA of control at P_{in}=1.0 bar.

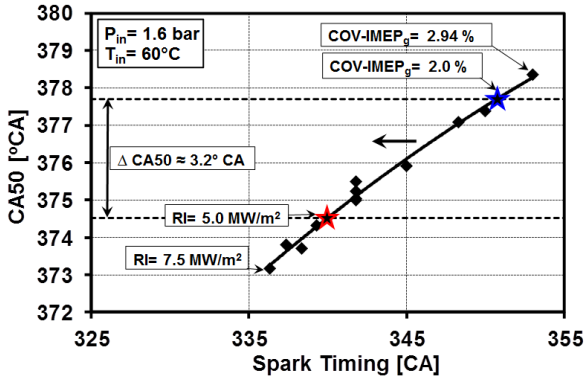

Figure 18. CA50 control sweep at P_{in}=1.6 bar, T_{in}= 60°C with EGR.

When analyzing the heat release rates for the control sweep at P_{in}=1.6 bar, the highest P_{in} for which SA data were acquired, some low-temperature heat release (LTHR) was observed, even though it was not observed at the lower P_{in}s, for which higher intake temperatures were used. This is illustrated in Figure 19, which shows HRRs for the RI=5 MW/m^2 and COV-IMEP$_g$ = 2.94% points shown on the CA50 control-sweep curve in Figure 18, along with the HRR for CI-only with COV-IMEP$_g$ = 5%. As can be seen, the LTHR occurs at nearly the same crank angle and is nearly the same magnitude for all three curves, indicating that the presence of the spark has little effect on the LTHR for these data. This is perhaps not surprising since the spark timing for the RI=5 MW/m^2 point occurs at the start of the LTHR, before there is time for significant flame propagation, so there is only a slight increase in the LTHR over the other two curves. For the SA COV-IMEP$_g$ = 2.94% point, the spark occurs after the LTHR is over, and the LTHR is identical to that of the CI-only point. Further investigation is needed to determine the extent to which SA can interact with the LTHR to influence the ability to use SA to improve LTGC operation.

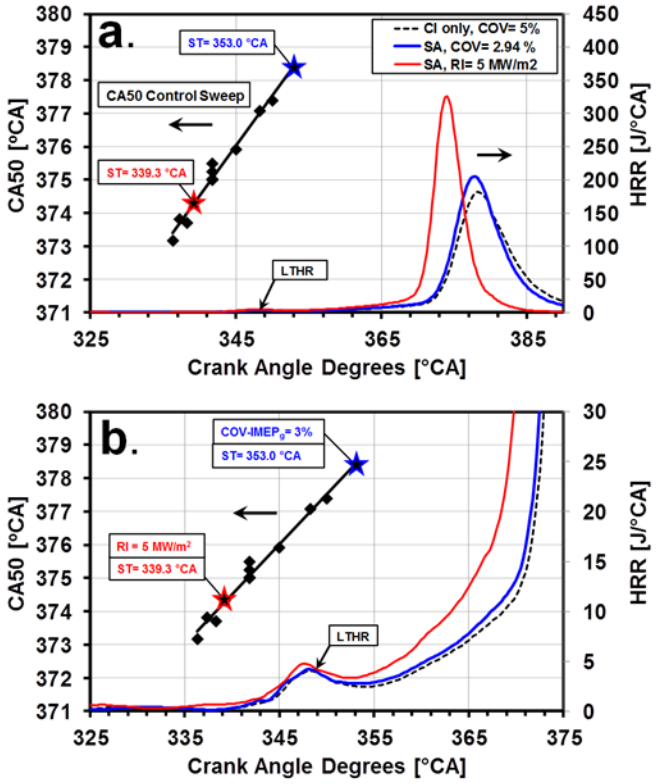

Figure 19. (a) Heat release rates that correspond to the CA50 control sweep at P_{in}=1.6 bar (b) Close-up view of the heat release rates showing the LTHR.

The effects of equivalence ratio on the EGR and spark timing requirements at P_{in}=1.6 bar are shown in Figure 20a. In this figure, the dashed lines show the baseline oxygen concentration that gave RI=3 MW/m^2 with CI-only, which defined the start of these sweeps. The ϕ_m=0.42 curve is the same data that was presented in Figure 16. When the equivalence ratio increases to ϕ_m=0.45 more EGR (a lower intake oxygen concentration) is needed to compensate for the hotter wall temperatures and hotter residuals that occur with the higher ϕ_m. For each ϕ_m, as the EGR was increased (O_2 concentration reduced), the spark timing had to be advance to compensate. As can be seen in Figure 20b, with ϕ_m=0.42 and ϕ_m=0.45 the EGR limit occurs when the COV-IMEP$_g$ increases greatly similar to what occurred at P_{in}=1.0 bar for these ϕ_ms, except that the rise in COV-IMEP$_g$ is not as rapid. There appears to be some partial burn cycles first before a complete misfire, causing the approach to COV-IMEP$_g$=2% to be more gradual.

For the lower equivalence ratios of ϕ_m=0.36 and ϕ_m=0.38, as the EGR level increased, the spark timing could be advanced without being accompanied by a significant rise in the COV-IMEP$_g$ regardless of the spark timing. However, when the spark timing was advanced before 330° CA, the EGR level had to be decreased in order to maintain RI=5 MW/m^2. Continuing to decrease the EGR level and advance the spark timing resulted in a flame that became progressively weaker, with the curves approaching the RI=3 MW/m^2 CI baseline.

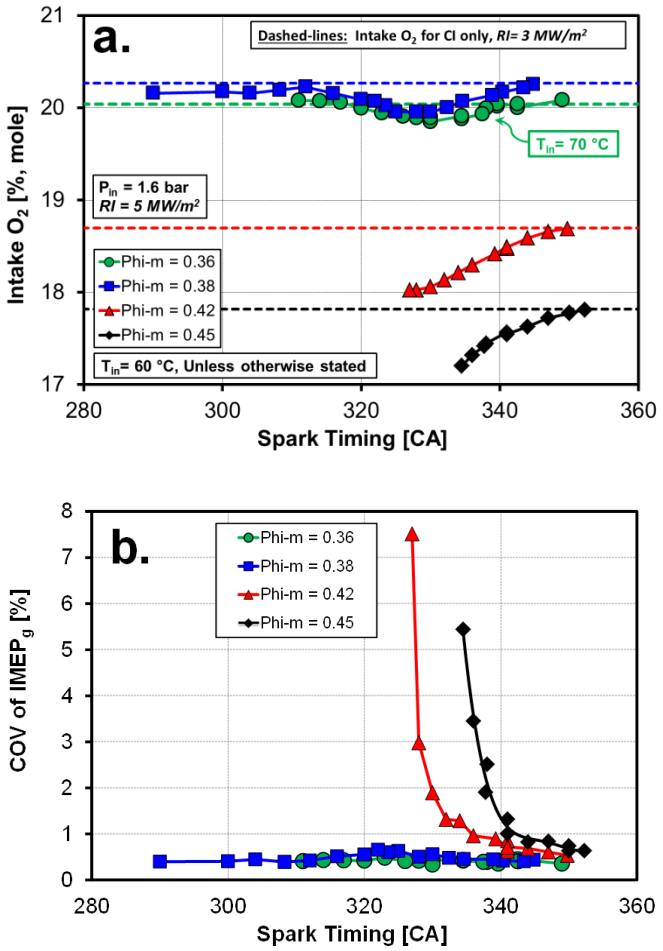

Figure 20. Equivalence ratio effects at P_{in}=1.6 bar and T_{in}= 60°C using EGR (a) EGR and Spark Timing sweep (b) Variation of COV-IMEP$_g$ with spark advance and EGR level.

Interestingly, the peak allowable ΔO_2 for ϕ_m=0.36 and ϕ_m=0.38 occurred with a spark timing near 330° CA, approximately the same spark timing when the ϕ_m=0.42 sweep became COV-IMEP$_g$ limited.

Taking a closer look at Figure 17, this COV-IMEP$_g$=2% limit is what appears to explain the decreasing trend in maximum ΔT_{in} with boost pressure. Based on our earlier results where we showed that the rapid rise in COV-IMEP$_g$ was due to a few misfire cycles, our working hypothesis was that that the cause of the misfired cycles might be related to the initial turbulent flame propagation.

To begin the analysis to investigate this further, we estimated the laminar burning velocity (S_L) for the last data points before COV-IMEP$_g$>2% using a set of correlations for premixed iso-octane, air, and EGR mixtures proposed by Middleton et al. [25]. These correlations were developed for conditions relevant to LTGC engines and include terms that account for the fuel concentration, oxygen concentration, and a characteristic

temperature for the flame chemistry (this term accounts for the effect of pressure on the burning velocity).

Figure 21 shows how the COV-IMEP$_g$=2% limits were defined in Figure 16. The last stable data points were chosen before the threshold when misfire cycles started to occur. The in-cylinder conditions and mixture properties corresponding to these points were then used to compute the laminar burning velocities for the entire cycle, with the results shown in Figure 22.

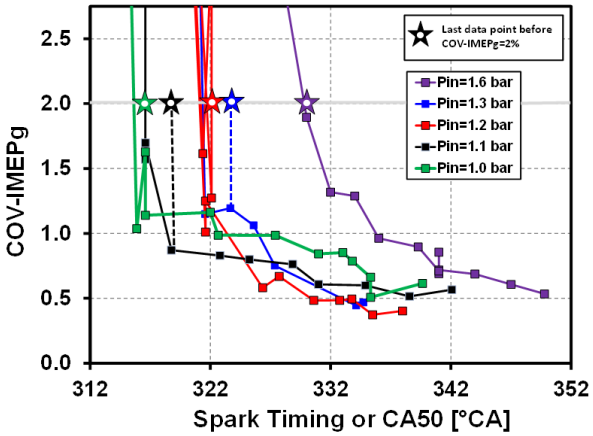

Figure 21. Illustration of the COV-IMEP$_g$=2% limits.

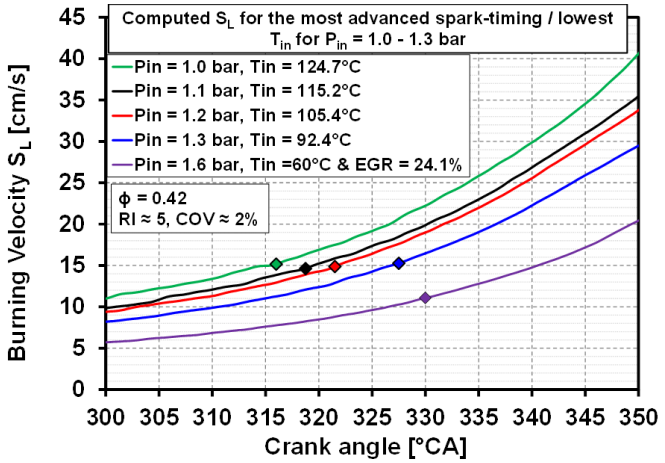

Figure 22. Computed laminar flame speeds for the conditions just before COV-IMEP$_g$>2%; data markers indicate the burning velocity at the time of the spark.

On this plot, data markers were added to indicate the laminar flame speeds at the time of the spark. Astonishingly, the laminar flame speeds at the time of the spark for P_{in}=1.0 to 1.3 bar turned out to be nearly the same at S_L=15 cm/s, perhaps implying some type of fundamental limit. Both higher intake pressures and higher pressures act to diminish the laminar flame speed, and it appears that the spark timing has to occur later in the cycle to establish a sufficient burning velocity, which was found to be S_L=15 cm/s for these conditions. For P_{in}=1.6 bar, the computed laminar flame speed is lower than the others. However, when interpreting the laminar burning velocity results, it's worth keeping in mind that the correlations are for iso-octane, which may not be representative of the actual fuel chemistry that occurs with gasoline (including the effects of LTHR), and particularly for gasoline-ethanol blends like RD5-87.

However, remarkably, the apparent limit to the laminar flame speed limit at S_L=15 cm/s shows excellent agreement with the results presented by Ayala and Heywood [26] in their study of combustion variability at the lean limits of an SI engine. For their experiments, the CR of the engine was 9.8:1 and the fuel used was indolene [26, 27]. An equivalence ratio sweep was performed at a constant load equal to 3.5 bar NIMEP, with the spark timing set to maximum brake torque conditions for all points. The equivalence ratios spanned from stoichiometric to about ϕ_m=0.58, when the combustion stability started to deteriorate (COV-NIMEP>2%). For the entire sweep, the laminar flame speed at the time of the spark was calculated using a correlation for indolene. Ayala and Heywood observed that as the equivalence ratio decreased, the trend in COV-NIMEP rose slowly at first, and then rapidly increased when the computed laminar flame speed was about 15 cm/s.

To understand the fundamental physics behind this limit, they applied a turbulent-flame propagation model [28]. In this model, the rate at which the mixture is burned is represented by a laminar burning component (which dominates early on), and a term that describes the rate at which entrained unburned-mass burns (which dominates as time progresses

and the flame becomes more developed). This characteristic time to burn an eddy of unburned mixture in this second term has an inverse dependence on the laminar flame speed; thus, very low laminar flame speeds cause the characteristic burning-time to become exceedingly long. Furthermore, the trend in percent change of this variable tracked well with the increase in percent change of COV-NIEMP, leading them to the conclusion that this relationship was why the COV-NIMEP began to rapidly increase at S_L=15 cm/s.

Although emissions measurements were not a primary focus of this study, the effects of intake pressure boost on indicated specific NO_x ($ISNO_x$) and the percent fuel carbon into unburned hydrocarbons (HC) and carbon monoxide (CO) are shown in Figures 23 and 24, respectively. For both CI and SA, $ISNO_x$ values are below the US 2010 Heavy Duty limit for all intake pressures. Generally, increasing intake boost decreases $ISNO_x$, and SA values are below or comparable to the measurements for CI.

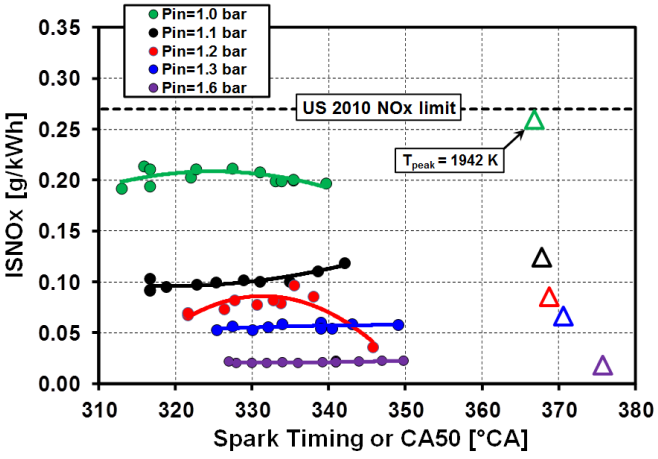

Figure 23. Effects of intake pressure-boost on NO_x emissions.

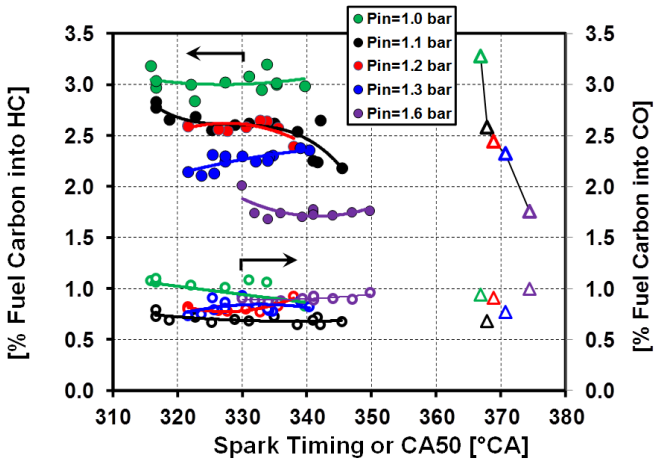

Figure 24. Percent fuel carbon into HC and CO emissions.

There seemed to be little correlation with intake pressure and CO emissions, with only about 0.5-1.0% of the fuel carbon going to CO emissions. However, there is a clear trend with HC emissions; increasing boost pressure results in a smaller percent of the fuel carbon going to unburned hydrocarbons. Furthermore, the HC measurements vary from about 1.75% to 3.25%, which is more significant than the CO measurements when computing combustion efficiency, which is shown in Figure 25a. Figure 25b shows the trend in thermal efficiency. Both thermal efficiency and combustion efficiency improve as intake pressure is increased. The improvement in thermal efficiency can be attributed to lower intake temperatures and the concomitant improvement in combustion efficiency as boost-pressure increases. Moreover, at a given P_{in}, the thermal efficiencies do not appear to increase significantly as T_{in} is decreased to its lowest values. This suggests that the early heat release associated with the flame combustion is offsetting any gains in thermal efficiency that are typically associated with lower intake temperatures.

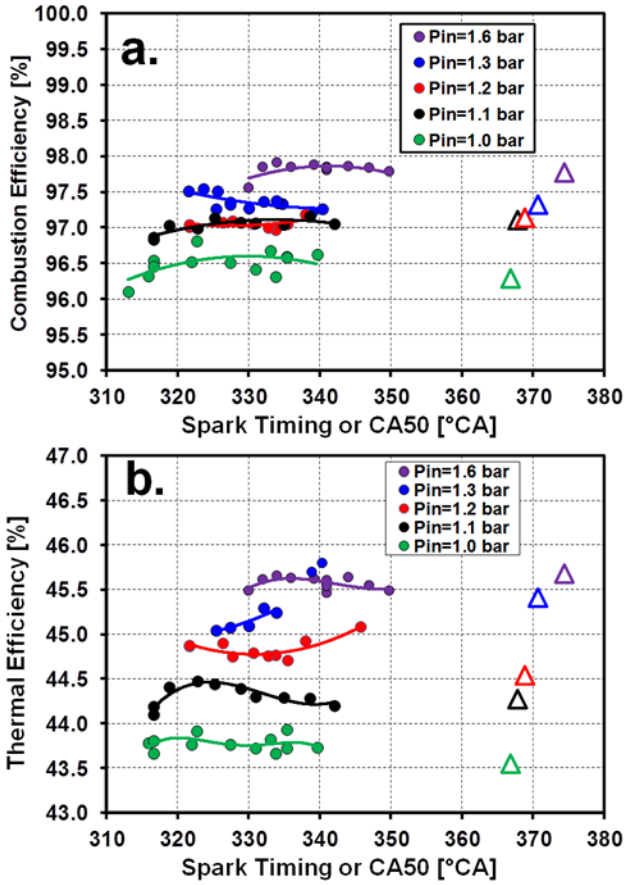

Figure 25. Trends in combustion efficiency and thermal efficiency with intake-pressure boost.

Summary and Conclusions

In this paper, fully premixed experiments were performed to study the ability to provide robust control with SA-LTGC by examining fundamental aspects such as the effects of changing compression ratio, fuel properties, equivalence ratio, and intake pressure. Two types of experimental sweeps were performed to study these effects.

The first type of sweep demonstrated the amount of CA50 control that was possible for different conditions. The intake temperature (or intake oxygen concentration when using EGR) was held constant, and the spark timing was varied to advance the combustion phasing to the onset of knocking (RI=5 MW/m^2), or even further to the point of heavy knocking (RI=7 MW/m^2), and then retarding the combustion phasing until the combustion stability started to deteriorate (COV-IMEP$_g$>2%). These sweeps showed that for a constant intake temperature, advancing the spark timing resulted in increasing amounts of compression heating from the flame propagation. Furthermore, retarding the spark timing from the onset of ringing (RI=5 MW/m^2) resulted in the ringing intensity decreasing and the combustion phasing becoming more retarded until COV-IMEP$_g$>2%, which occurred without any misfires.

The second type of sweep showed the ability of SA to operate with substantially lower intake temperatures, by using compression heating from the flame propagation to compensate for the reduced intake temperature. The maximum allowable ΔT_{in} was defined as the difference between the intake temperature obtained with CI at RI=5 MW/m^2 and the lowest allowable temperature before COV-IMEP$_g$ > 2%. For these sweeps, the spark timing was set to provide RI=5MW/m^2, and as the intake temperature was incrementally decreased, the spark timing was advanced to maintain RI=5MW/m^2. For P_{in}=1.0-1.3 bar, the allowable decrease in intake temperature was limited by a sudden rise in COV-IMEP$_g$, determined to be caused by a few misfire cycles. However, at P_{in}=1.6 bar the approach to the COV-IMEP$_g$ limit was more gradual, with some partial burn cycles occurring instead of complete misfires.

Some of the main findings of this study are listed below:

- ϕ_m=0.42 was found to be near the optimal equivalence ratio for the maximum amount of ΔT_{in}, at both P_{in}=1.0 bar and P_{in}=1.6 bar.
- At P_{in}=1.0 bar, the amount of CA50 control between the limits of RI=5 MW/m^2 and COV-IMEP$_g$=2% was comparable for ϕ=0.38 and 0.42, with slightly less CA50 control with increasing ϕ_m. However, with ϕ=0.38 the RI never exceeded 4 MW/m^2 due to reduced compression heating from the propagating flame.
- ϕ_m=0.36 was the lowest ϕ_m for a spark-initiated flame to provide sufficient compression heating to affect the autoignition of the main portion of the charge. Thus, some form of stratification would be required to apply spark assist to conditions where the global ϕ_m<0.36.
- At naturally aspirated conditions, the maximum ΔT_{in} using different fuels (CF-E0 and RD5-87) and compression ratios (CR=14:1 and CR=16:1) were nearly identical, at about ΔT_{in}=21°C.
- For analogous T_{in}'s corresponding to COV-IMEP$_g$ = 5% with CI-only, the maximum ΔCA50 at CR=14:1 using RD5-87 was 5.4° CA, about 1° CA less than what could be achieved at CR=16:1 using CF-E0. However, using CR=14:1 and RD5-87 provided slightly more control when the T_{in} was lowered 10°C, with 3.0° CA of control, compared to 2.3° CA using CR=16:1 and CF-E0.
- The maximum amount of ΔT_{in} decreased with increasing intake pressure boost, with the trend correlating well with the intake temperature and spark timing at the COV-IMEP$_g$=2% limits.
- For the spark timing at the COV-IMEP$_g$=2% limits, a computed laminar flame speed of S_L=15 cm/s was found for P_{in}=1.0-1.3 bar, possibly implying a fundamental limit to the flame propagation.
- Using RD5-87, between the limits of RI=5 MW/m^2 and COV-IMEP$_g$=2%, only 3.2° CA of control was possible at P_{in}=1.6 bar compared to 6.5° CA of control at P_{in}=1.0 bar.
- ISNO$_x$ values were found to be below the US-2010 limits, and decreased with increasing intake pressure. Similarly, HC emissions decreased with intake boost, but little correlation with intake pressure was found for CO emissions.
- With SA, NO$_x$ emissions were similar to or slightly below the CI-only point at the same ϕ_m and P_{in}. HC and CO emissions with SA were generally similar to the comparable CI-only point.

Contact Information

Corresponding author:

John E. Dec
Sandia National Laboratories
MS 9053, PO Box 969
Livermore, CA 94551-0968, USA

Acknowledgements

The authors would like to thank Tim Gilbertson, Keith Penney, Gary Hubbard, and Alberto Garcia for their dedicated support of the LTGC Engine Laboratory.

This work was performed at the Combustion Research Facility, Sandia National Laboratories, Livermore, CA, Support was provided by the U.S. Department of Energy, Office of Vehicle Technologies. Sandia National Laboratories is a multi-mission laboratory managed and operated by National Technology and Engineering Solutions of Sandia, LLC., a wholly owned subsidiary of Honeywell International, Inc., for the U.S. Department of Energy's National Nuclear Security Administration under contract DE-NA0003525.

Definitions/Abbreviations

aTDC	after top dead center
AHRR	apparent heat release rate
AKI	Anti-Knock Index = (RON + MON)/2
BDC	bottom dead center
bTDC	before top dead center
CA	crank angle
CAD	crank angle degrees
°CA	crank angle degrees
CA50	crank angle of 50% burn point
CF-E0	Haltermann certification gasoline containing zero ethanol. Specification in Table 2.
CI	compression ignition
CR	compression ratio
CO	carbon monoxide
CO_2	carbon dioxide
COV	coefficient of variation
DI	direct injection
DHA	detailed hydrocarbon analysis
E10	10% Ethanol
EGR	exhaust gas recirculation
GDI	gasoline direct injector
HC	hydrocarbon
HCCI	homogeneous charge compression ignition – a well premixed form of LTGC
HRR	heat release rate
$IMEP_g$	gross indicated mean effective pressure
ISNOx	indicated specific NOx
LTGC	low temperature gasoline combustion
MON	Motor Octane Number
NIMEP	net indicated mean effective pressure
O_2	oxygen
P_{in}	intake pressure
PLIF	Planar Laser Induced Fluorescence
PM	particulate matter
PRR	pressure rise rate
PPRR	peak pressure rise rate
RD5-87	research-quality, regular-grade E10 gasoline. Specifications in Table 2.
RI	ringing intensity, see Eq. 2
RON	research octane number
RPM	revolutions per minute
SL	laminar flame speed
SA	spark assist
T_{in}	intake temperature
ΔT_{in}	The difference between the T_{in} obtained with CI at RI=5 MW/m^2 and the lowest allowable T_{in} before COV-$IMEP_g$ > 2%.
TDC	top dead center
NO_x	oxides of nitrogen

References

1. Dec, John E. 2014. "Advanced Compression-Ignition Combustion for High Efficiency and Ultra-Low NOX and Soot." In *Encyclopedia of Automotive Engineering*. John Wiley & Sons, Ltd.
2. Yun, Hanho, Nicole Wermuth, and Paul Najt. 2011. "High Load HCCI Operation Using Different Valving Strategies in a Naturally-Aspirated Gasoline HCCI Engine." *SAE International Journal of Engines* no. 4 (1):1190-1201. doi: 10.4271/2011-01-0899.
3. Persson, H., A. Hultqvist, B. Johansson, and A. Remón. 2007. Investigation of the Early Flame Development in Spark Assisted HCCI Combustion Using High Speed Chemiluminescence Imaging. SAE International.
4. Persson, H., R. Pfeiffer, A. Hultqvist, B. Johansson, and H. Ström. 2005. Cylinder-to-Cylinder and Cycle-to-Cycle Variations at HCCI Operation With Trapped Residuals. SAE International.
5. Zigler, B. T., P. E. Keros, K. B. Helleberg, M. Fatouraie, D. Assanis, and M. S. Wooldridge. 2011. "An experimental investigation of the sensitivity of the ignition and combustion properties of a single-cylinder research engine to spark-assisted HCCI." *International Journal of Engine Research* no. 12 (4):353-375. doi: 10.1177/1468087411401286.
6. Manofsky, Laura, Jiri Vavra, Dennis N. Assanis, and Aristotelis Babajimopoulos. 2011. Bridging the Gap between HCCI and SI: Spark-Assisted Compression Ignition. SAE International.
7. Foong, Tien Mun, Kai J. Morganti, Michael J. Brear, Gabriel da Silva, Yi Yang, and Frederick L. Dryer. 2014. "The octane numbers of ethanol blended with gasoline and its surrogates." *Fuel* no. 115 (Supplement C):727-739. doi: https://doi.org/10.1016/j.fuel.2013.07.105.
8. Olesky, Laura K. Manofsky, Robert J. Middleton, George A. Lavoie, Margaret S. Wooldridge, and Jason B. Martz. 2015. "On the sensitivity of low temperature combustion to spark assist near flame limit conditions." *Fuel* no. 158 (Supplement C):11-22. doi: https://doi.org/10.1016/j.fuel.2015.05.012.
9. Olesky, Laura Manofsky, George A. Lavoie, Dennis N. Assanis, Margaret S. Wooldridge, and Jason B. Martz. 2014. "The effects of diluent composition on the rates of HCCI and spark assisted compression ignition combustion." *Applied Energy* no. 124 (Supplement C):186-198. doi: https://doi.org/10.1016/j.apenergy.2014.03.015.
10. Olesky, Laura Manofsky, Jason B. Martz, George A. Lavoie, Jiri Vavra, Dennis N. Assanis, and Aristotelis Babajimopoulos. 2013. "The effects of spark timing, unburned gas temperature, and negative valve overlap on the rates of stoichiometric spark assisted compression ignition combustion." *Applied Energy* no. 105 (Supplement C):407-417. doi: https://doi.org/10.1016/j.apenergy.2013.01.038.
11. Dec, John E., Yi Yang, and Nicolas Dronniou. 2012. "Improving Efficiency and Using E10 for Higher Loads in Boosted HCCI Engines." *SAE International Journal of Engines* no. 5 (3):1009-1032. doi: 10.4271/2012-01-1107.
12. Dronniou, Nicolas, and John E. Dec. 2012. "Investigating the Development of Thermal Stratification from the Near-Wall Regions to the Bulk-Gas in an HCCI Engine with Planar Imaging Thermometry." *SAE International Journal of Engines* no. 5 (3):1046-1074. doi: 10.4271/2012-01-1111.
13. Zhao, Fu-Quan, Ming-Chia Lai, and David L. Harrington. 1995. The Spray Characteristics of Automotive Port Fuel Injection-A Critical Reviews. SAE International.
14. Styron, J. P., P. L. Kelly-Zion, C. F. Lee, J. E. Peters, R. A. White, and R. P. Lucht. 2000. Multicomponent Liquid and Vapor Fuel Distribution Measurements in the Cylinder of a Port-Injected, Spark-Ignition Engine. SAE International.
15. Dec, John E., and Yi Yang. 2010. "Boosted HCCI for High Power without Engine Knock and with Ultra-Low NOx Emissions - using Conventional Gasoline." *SAE International Journal of Engines* no. 3 (1):750-767. doi: 10.4271/2010-01-1086.
16. Yang, Yi, John E. Dec, Nicolas Dronniou, and William Cannella. 2012. "Boosted HCCI Combustion Using Low-Octane Gasoline with Fully Premixed and Partially Stratified Charges." *SAE International Journal of Engines* no. 5 (3):1075-1088. doi: 10.4271/2012-01-1120.
17. Dec, John E., Jeremie Dernotte, and Chunsheng Ji. 2017. "Increasing the Load Range, Load-to-Boost Ratio, and Efficiency of Low-Temperature Gasoline Combustion (LTGC) Engines." *SAE International Journal of Engines* no. 10 (3):1256-1274. doi: 10.4271/2017-01-0731.
18. Dernotte, Jeremie, John Dec, and Chunsheng Ji. 2017. Efficiency Improvement of Boosted Low-Temperature Gasoline Combustion Engines (LTGC) Using a Double Direct-Injection Strategy. SAE International.
19. Dec, John E., Yi Yang, Jeremie Dernotte, and Chunsheng Ji. 2015. "Effects of Gasoline Reactivity and Ethanol Content on Boosted, Premixed and Partially Stratified Low-Temperature Gasoline Combustion (LTGC)." *SAE International Journal of Engines* no. 8 (3):935-955. doi: 10.4271/2015-01-0813.
20. Dernotte, Jeremie, John E. Dec, and Chunsheng Ji. 2015. "Energy Distribution Analysis in Boosted HCCI-like / LTGC Engines - Understanding the Trade-Offs to Maximize the Thermal Efficiency." *SAE International Journal of Engines* no. 8 (3):956-980. doi: 10.4271/2015-01-0824.
21. Dec, John E., and Magnus Sjöberg. 2003. A Parametric Study of HCCI Combustion - the Sources of Emissions at Low Loads and the Effects of GDI Fuel Injection. SAE International.
22. Heywood, John B. 1988. *Internal combustion engine fundamentals*: New York : McGraw-Hill, [1988] ©1988.
23. Eng, J. A. 2002. Characterization of Pressure Waves in HCCI Combustion. SAE International.
24. Sjöberg, Magnus, John E. Dec, Aristotelis Babajimopoulos, and Dennis N. Assanis. 2004. Comparing Enhanced Natural Thermal Stratification Against Retarded Combustion Phasing for Smoothing of HCCI Heat-Release Rates. SAE International.

25. Middleton, Robert J., Jason B. Martz, George A. Lavoie, Aristotelis Babajimopoulos, and Dennis N. Assanis. 2012. "A computational study and correlation of premixed isooctane air laminar reaction fronts diluted with EGR." *Combustion and Flame* no. 159 (10):3146-3157. doi: https://doi.org/10.1016/j.combustflame.2012.04.014.
26. Ayala, Ferrán A., and John B. Heywood. 2007. Lean SI Engines: The role of combustion variability in defining lean limits. Consiglio Nazionale delle Ricerche, DOI: https://doi.org/10.4271/2007-24-0030
27. Ayala, Ferrán A., Michael D. Gerty, and John B. Heywood. 2006. Effects of Combustion Phasing, Relative Air-fuel Ratio, Compression Ratio, and Load on SI Engine Efficiency. SAE International.
28. Tabaczynski, Rodney J., Frederick H. Trinker, and Ben A. S. Shannon. 1980. "Further refinement and validation of a turbulent flame propagation model for spark-ignition engines." *Combustion and Flame* no. 39 (2):111-121. doi: https://doi.org/10.1016/0010-2180(80)90011-5.

APPENDIX

Figure A.1 shows how ΔO_2 is equivalent to $\Delta T_{in,}$ which was determined by performing the following experiment. First, by holding the intake temperature at 70°C, an oxygen concentration of 18.5% was found to give RI=5.0 MW/m^2. By increasing the EGR level, the O_2 concentration was then decreased until RI=2.5 MW/m^2. The RI=5.0 MW/m^2 data point was then repeated, and this time the oxygen concentration was held constant while decreasing T_{in} until RI=2.5 MW/m^2. Extrapolating, it was found that 0.3% ΔO_2 scaled with every 5°C of ΔT_{in}.

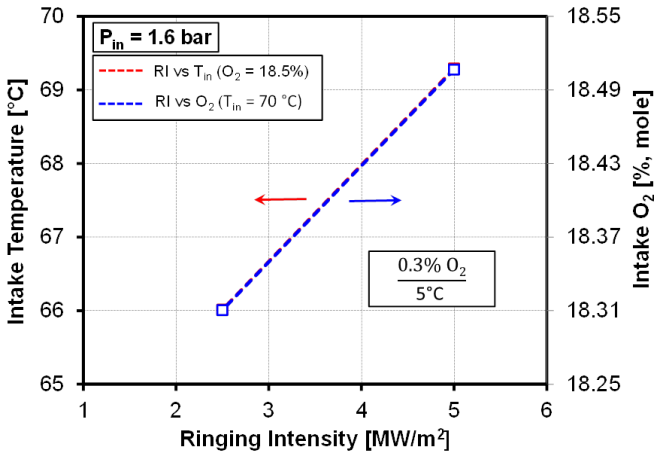

Figure A.1. Conversion from ΔO_2 to an equivalent ΔT_{in}